

Can power-law scaling and neuronal avalanches arise from stochastic dynamics?

Jonathan Touboul^{1,2,*}, Alain Destexhe³,

1 Department of Mathematics, University of Pittsburgh, Pittsburgh PA, USA

2 Laboratory of Mathematical Physics, The Rockefeller University, New York, NY USA

3 Unité de Neurosciences Intégratives et Computationnelles (UNIC), UPR CNRS 2191, 91198 Gif-sur-Yvette, France.

* E-mail: jonathan.touboul@gmail.com

December 9, 2018

Abstract

The presence of self-organized criticality in biology is often evidenced through the power-law scaling of event size distributions represented in logarithmic scale. We show here that such a procedure does not necessarily mean that the system exhibits power-law scaling. We first provide an analysis of multisite local field potential (LFP) recordings of brain activity and show that event size distributions defined as negative LFP peaks can be close to power-law distributions. This result is however not robust to change in detection threshold, or to more severe statistical analyses such as the Kolmogorov-Smirnoff test. Similar power-law scaling is observed for surrogate signals, suggesting that power-law scaling may be a generic property of thresholded stochastic processes. We next investigate this problem analytically and show that indeed, spurious power-law scaling can appear from stochastic processes without the presence of underlying self-organized criticality. However, this power-law is only apparent in logarithmic representations, but does not resist to more severe analysis such as the Kolmogorov-Smirnoff test. We conclude that logarithmic representations can lead to spurious power-law scaling induced by the stochastic nature of the phenomenon, and should be demonstrated by more stringent statistical tests.

Introduction

The presence of self-organized criticality was shown for several biological systems, including spontaneous brain activity *in vitro* (Beggs and Plenz 2004) which displays spontaneous bursts of activity – or “neuronal avalanches” – separated by silences. The distribution of such events was clearly scaling as a power-law, which constitutes evidence for self-organized criticality in this system (see also review by Jensen (1998)).

To investigate if criticality is important for brain function, the same type of analysis was also investigated *in vivo*, and in particular in awake animals. However, the difficulty with such analyses is that the activity in awake animals is much more intense compared to *in vitro* (Steriade 2001), with often no visible “pause” in the firing activity, which complicates the definition of avalanches. In a first study on awake cats (Bedard et al. 2006), it was shown that macroscopic variables such as the extracellular local field potential (LFP) show $1/f$ scaling in power spectra, but the underlying neuronal activity did not show signs of criticality. In a second, more recent study on awake monkeys (Petermann et al. 2009), power-law scaling was apparent from LFPs when considering negative peaks, which are known to be related to neuronal firing. This scale-invariant behavior was taken as evidence for self-organized criticality.

In the present paper, we attempt to resolve these contradictory observations by first performing the same analysis on negative LFP peaks in cats, and then consider different statistical tests and models to explain these observations. We study the statistical distribution of avalanche sizes, as well as negative peaks in the LFPs (linked to neuronal firings), positive peaks and surrogate data. We then turn to study similar stochastic problems and show to what extent the results obtained by the experimental data analysis can also be observed in purely stochastic systems without the presence of underlying self-organized criticality.

Material and Methods

In this section, we review theoretical methods to assess and quantify power-law and exponential scalings of experimental and simulated data, as used in the rest of the article.

Identifying tail distributions

Power-law and exponential distributions

Mathematically, a random variable X is said to present a power law distribution if it is drawn from a probability distribution with density:

$$\mathbb{P}(x \leq X \leq x + dx) = a x^{-\alpha} dx \quad (1)$$

where α is a constant parameter of the distribution known as the *exponent* or *scaling* parameter. In practice, few empirical phenomena obey power laws for all values of x , and in general power laws characterize the tail of the distribution, i.e. the probability distribution of values of X greater than some value x_{\min} . In such cases we say that the tail of the distribution follows a power law.

Power-law relations characterize an important number of physical, biological and economical phenomena, and is particularly interesting for the scale invariance it presents. More precisely, let $p(x)$ be the power-law density given by 1. Given the relation $p(x) = ax^{-\alpha}$, scaling x by a constant factor yields to a proportional law: $p(cx) = ac^{-\alpha}x^{-\alpha}$. Another notable property is the universality of power-laws in physical phenomena such as phase transitions in physics. In these cases, the exponent is called the critical exponent. Diverse systems as they approach criticality, can be shown to share the same fundamental dynamics.

In this paper we are interested in discriminating power-laws with another type of statistics, the exponentially-tailed distribution. Such random variables are characterized for $x \geq x_{\min}$ by an exponential probability density:

$$\mathbb{P}(x \leq X \leq x + dx) \sim Ce^{-\lambda x} dx \quad (2)$$

Given some experimental data, the problem is now to identify the parameters of the best-fitted power-law or exponential law, which means estimating the parameter \hat{x}_{\min} and the power-law exponent $\hat{\alpha}$ or the exponential-law intensity $\hat{\lambda}$.

Parameter evaluations

Taking the logarithm of the probability density of a power-law random variable, we obtain $\log(p(x)) = -\alpha \log(x) + \log(a)$. The histogram of the power-law therefore presents an affine relation in a log-log plot. Similarly, the exponential distribution's histogram is characterized by an affine relation in a log-linear plot. For this reason, power-laws in empirical data are often studied plotting the logarithm of the histogram as a function of the logarithm of the values of the random variable, and doing a linear regression, mostly using a least-square algorithm to best fit an affine line through the data points. This methods dates back to Pareto in the 19th century (see e.g. Arnold (1983)). The evaluated point \hat{x}_{\min} corresponding to the point where the data start having a power-law distribution is mostly evaluated visually, but this method is very sensitive to noise, fluctuations is subjective (see e.g. Stoev et al. (2006) and references herein). However, this widely used technique, as well as other variations on the same page generate systematic errors under relatively common conditions (see e.g. Clauset et al. (2009)). Moreover, there is not any evaluation of the goodness of fit obtained by the power law assumption.

In this paper we prefer to use a maximum likelihood estimator, which is considered the most reliable of usual estimators (see Clauset et al. (2009) for a comparison of different estimators). It is known to

provide an accurate parameter estimate in the limit of large sample size (see Barndorff-Nielsen and Cox (1995); Muniruzzaman (1957)).

Assume that the starting value above which the tail of the distribution x_{\min} is known. Then the expressions of the maximum likelihood estimator and maximal likelihood are well known and read for the power-law distribution, for $x_i \geq x_{\min}$ and n the number of such data points:

$$\hat{\alpha} = 1 + n \left(\sum_{i=1}^n \log \frac{x_i}{x_{\min}} \right),$$

and for the exponential distribution:

$$\hat{\lambda} = n \sum_{i=1}^n n(x_i - x_{\min}).$$

The log-likelihood corresponding to this parameter value and the data reads in the case of the power-law distribution:

$$L(\hat{\alpha}|X) = n \log \left(\frac{\hat{\alpha} - 1}{x_{\min}} \right) - \hat{\alpha} \sum_{i=1}^n n \log \left(\frac{x_i}{x_{\min}} \right)$$

and in the case of the exponential law:

$$L(\hat{\lambda}|X) = n \log(\hat{\lambda}) - \hat{\lambda} \sum_{i=1}^n x_i.$$

The estimated parameter \hat{x}_{\min} is then by minimizing the Kolmogorov-Smirnoff value corresponding to the value:

$$D = \max_{x \geq x_{\min}} |S(x) - P(x)|$$

with $S(x)$ the cumulative distribution function of the data and $P(x)$ the theoretical power-law CDF that best fit the data for $x \geq x_{\min}$. The CDF functions are well known in statistics.

Goodness-of-fit and p-value validation

Given a data set, we now know how to evaluate the best power-law and best exponential-law fits. A direct comparison of the Kolmogorov-Smirnoff value gives the law explaining the best the data. But is this fit plausible and accurate? In order to answer this question, we use the standard goodness-of-fit test which generates a p -value quantifying the plausibility of the hypothesis. This method consists in generating different artificial samples of the estimated law, and compare the Kolmogorov-Smirnoff test with the value it has on the data set. The proportion of artificial data having a poorer fit than the original dataset is the p value. When this value is close to 1, the data set can be considered to be drawn from the law, and if not, the hypothesis might be rejected. The smallest p -values often considered to validate the statistical test are taken between 0.1 and 0.01.

Experimental Data

The experimental data used in the analysis consist of simultaneous recordings of multisite local field potentials (LFPs) and unit activity in the parietal cortex of awake cats (see Fig. 1), which was obtained from a previous study (Destexhe et al. 1999).

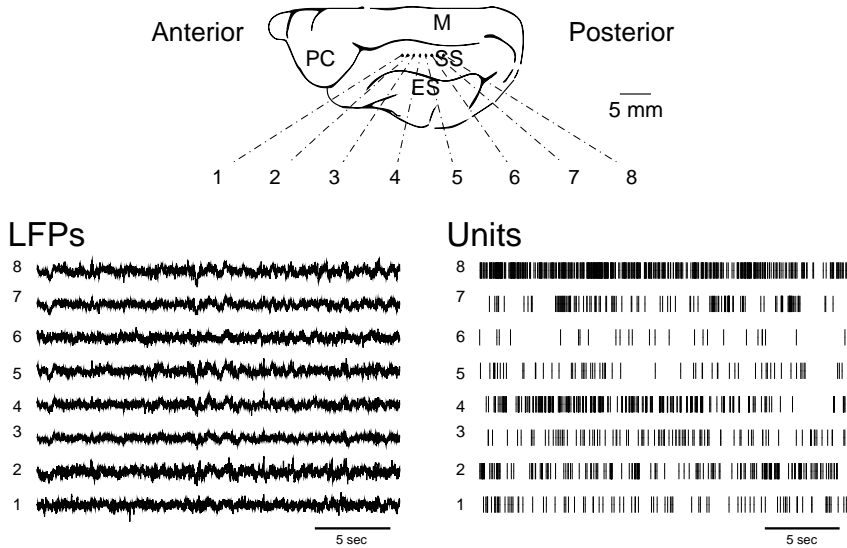


Fig. 1. Simultaneous multisite LFP and unit recordings in awake cats. Eight pairs of tungsten electrodes were inserted in cat cerebral cortex (area 5-7, parietal) as described in detail in Destexhe et al. (1999). The system (placement illustrated on top) recorded simultaneously LFPs (left) and raster plots of multi-unit activity (right) at each pair of electrode.

Results

Power-law scaling from LFPs in cerebral cortex

We start by analyzing the power-law scaling from experimental data. To analyze the power-law relations from LFP activity, we exploited the well-known relation between negative LFP peaks and neuronal firing. We proceeded to the detection of the negative peaks of the LFPs, called nLFPs, as shown in Fig. 2. The detection was done numerically using a fixed threshold, after digital filtering of the low-frequency (below 15 Hz) components of the signal and the detected peaks were then repositioned in the intact original signal (see the results of this detection for two different thresholds in Fig. 2 (top)). The detected LFP negative peaks were shown to be clearly related to neuronal firing by computing a wave-triggered average (WTA) of the unit activity. Indeed, at the times of detected peaks the average unit activity presented a clear increase, related to the presence of negative peaks of the LFP (Fig. 2, middle). The same procedure was repeated for all channels, leading to rasters of nLFP activity (Fig. 2, bottom).

We next performed an avalanche analysis based on the occurrence of nLFPs. Avalanches were defined by binning the raster of nLFPs according to time bins Δt (varied between 4 and 16 ms), and defining avalanches as clusters of activity among electrodes, separated by silent periods (time bins with no activity), in accordance with previous studies (Beggs and Plenz 2004; Petermann et al. 2009). The “size” of each avalanche was defined as the pooled amplitudes of all LFP peaks that define the avalanche. Using this procedure, the scaling of nLFP avalanche size distributions is shown in Fig. 3, for the two thresholds considered above. For high threshold, the avalanche distribution was better fit by a power-law, whereas for low threshold it appeared to fit more closely an exponential distribution. Similar results were obtained when the size was defined as the total number of events (peaks) within each avalanche (not shown). This shows that the exact functional form of the distribution highly depends on the peak detection threshold. Using a high detection threshold may give the impression of a power-law relation, but lowering the threshold makes the system tend to an exponential distribution, consistent with the exponential scaling of avalanches calculated from unit activity (Bedard et al. 2006).

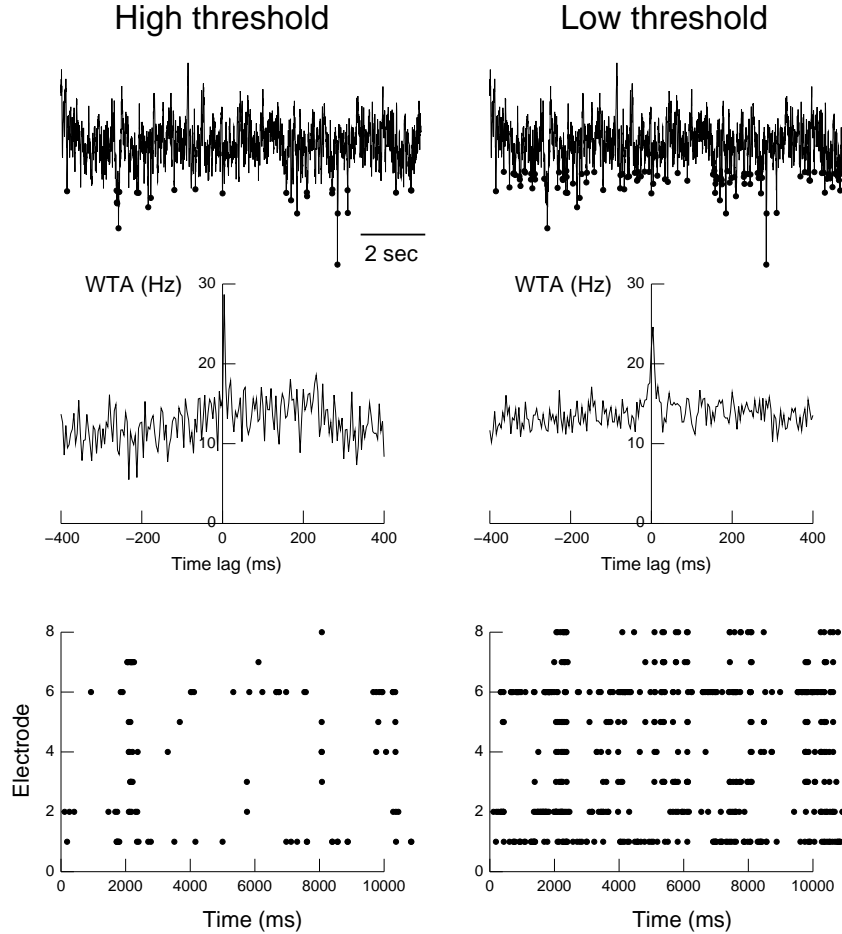


Fig. 2. Detection of negative peaks in local field potentials and their relation with neuronal activity. Top: detection of negative LFP peaks. The LFP signal is shown together with the detected nLFPs (circles). Middle: nLFP-based wave-triggered average (WTA) of unit activity, showing that the negative peaks were associated with an increase of neuronal firing. Bottom: rasters of nLFP activity. The same procedure is compared for high threshold (left panels) and low threshold (right panels).

To assess the significance of this result, we performed a Kolmogorov-Smirnoff test (see Section) to the same data. The results of this test are presented in Table 1 for avalanches defined from the cumulated peak amplitudes. We observe that the distribution of peak amplitudes is globally well fit by an exponential distribution, which is valid for a large proportion of the data. Indeed, an exponential fit yields significant p-values for both low and high threshold. Moreover, the estimated parameters for exponential fit hardly change when the threshold is varied, suggesting again that the observed exponential fit is meaningful. On the other hand, the estimated power-law parameters change significantly when changing the detection threshold and present a relatively low gof and high p-value tests, but account for very few data in the low threshold case. Thus, although the power-law distribution seems to provide a good fit if considered only by a linear regression in a log-log graphical representation, this apparent good fit is not supported by the statistical analysis, which suggests that the peak size distribution is globally better fit by an exponential distribution.

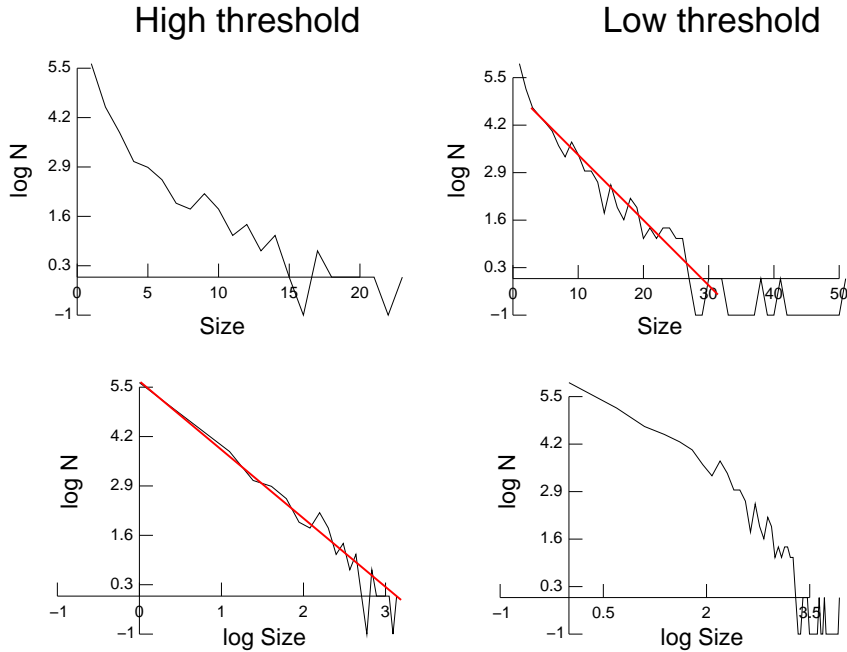


Fig. 3. Avalanche analysis of nLFPs in the awake cat. The nLFP avalanche size distributions were computed according to an avalanche analysis (see text). With high threshold, the avalanche distribution is better fit by a power-law (left panels); while it is better explained by an exponential distribution with low threshold (right panels).

Table 1. Kolmogorov-Smirnoff test on avalanche data

Data Type and threshold	Exponential fit				Power-Law fit			
	λ	gof	p-val	%	α	gof	p-val	%
Neg. Low	.18	0.028	0.07	38	5.32	0.050	0.94	4
Neg. High	0.13	0.042	0.07	20	2.01	0.077	0	88
Pos. Low	0.079	0.052	0	2.7	2.97	0.041	0.70	9
Pos High	0.18	0.033	0.27	31	1.93	0.091	0	93

Kolmogorov-Smirnoff test on avalanche analysis performed on positive (Pos) and negative (Neg) LFP peaks detected with a Low or High threshold. In this analysis, the avalanche size was the total cumulated amplitude of all LFP peaks within the avalanche. The λ is the estimated exponential parameter, the gof is the goodness-of-fit value. The smaller the gof, the better the fit. The closer to 1 the p-value, the better the fit. The % represents the percentage of data explained by the best fit. We observe that the distribution of these data is better represented by an exponential fit, and the positive peaks with a low threshold are not well modeled, neither by exponential laws nor by power laws.

It must be noted that another possible interpretation to the exponential scaling is that the low threshold condition adds a lot of spurious peaks, while still keeping a global relation with unit firing (Fig. 2, middle right). In this case, the spurious peaks give an exponential trend to the distribution, and the exponential scaling would thus be artifactual. In agreement with this, the WTA in Fig. 2 shows a weaker relation with unit firing for low threshold compared to high threshold. Thus, additional analyses

are needed to distinguish which of the power-law or exponential scaling is the one related to neural activity.

To further test the dependence on unit activity, we have repeated the same avalanche analysis, but using positive peaks of the LFP (Fig. 4A). In this case, as expected, the peaks are not related to unit firing (Fig. 4B). Unexpectedly, however, the scaling relations observed in graphical representations are similar as for nLFPs (Fig. 4C): both power-law and exponential law fit well the low-threshold data and exponential law better fits high threshold peaks. The statistical test reveals a power-law for low-threshold peaks and an exponential law for high threshold peaks. Interestingly, there are also some regions where the high threshold distributions scale exponentially and the low threshold condition displays exponential scaling (Fig. 4C, dotted lines). Here, the Kolmogorov-Smirnov test gave results very close to the case of negative peaks. Thus, similar to negative peaks, the apparent good fit of the power-law distribution is not supported by the statistical analysis.

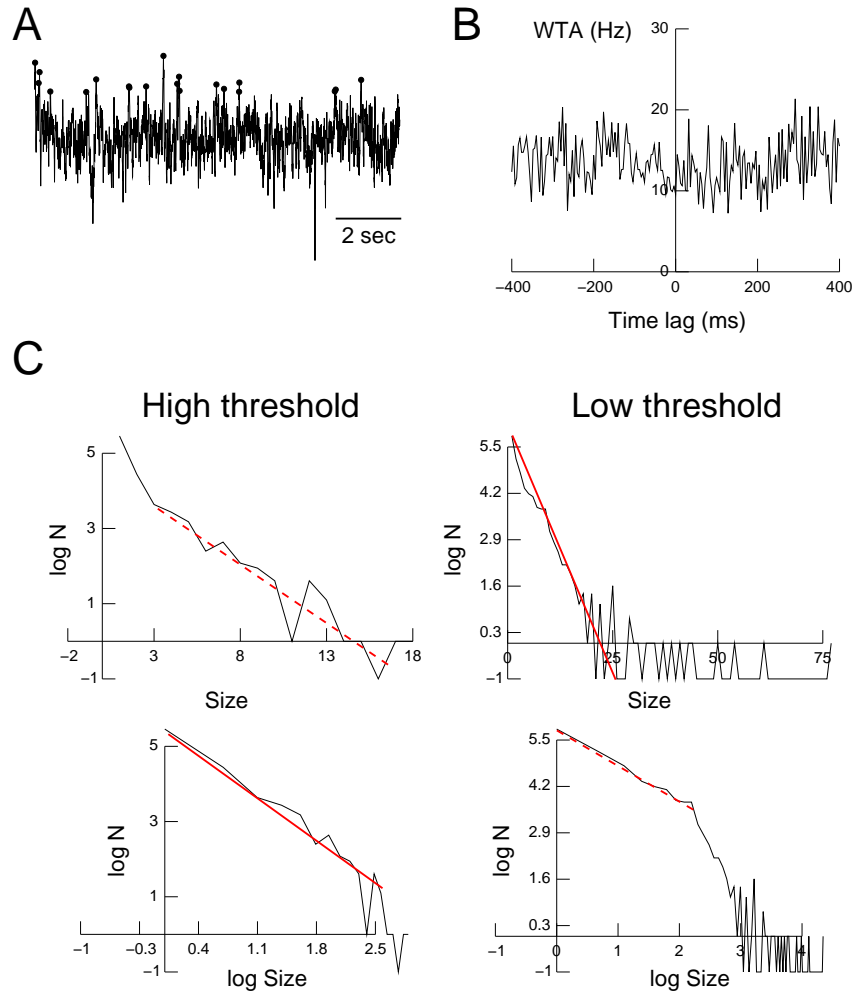


Fig. 4. Avalanche analysis from positive LFP peaks. A. Detection of positive LFP peaks using identical procedures as for nLFPs. B. Absence of relation of positive peaks with unit activity. C. Scaling of avalanche size distribution, showing similar behavior as for nLFPs (compare with Fig. 3).

Another essential test is to generate surrogate data sets. This was realized by taking the nLFP data sets, and randomly shuffling the occurrence times of the different peaks, but keeping the same distribution of peak amplitudes. The occurrence times were replaced by random numbers taken from a flat distribution. The avalanche analysis was then repeated from these randomized events, and the result is shown in Fig. 5. There is evidently no correlation between these peaks and unit activity, but interestingly, the same relations as above still persist. In particular, it is quite unexpected that such a stochastic system seems to give power-law distributed avalanche sizes. This power-law scaling was seen mostly for high threshold, while the low-threshold condition behaved more exponentially. The opposite scaling was also seen in restricted regions (Fig. 5C, dotted lines). The statistical tests realized on these surrogate data gave similar results as above (not shown).

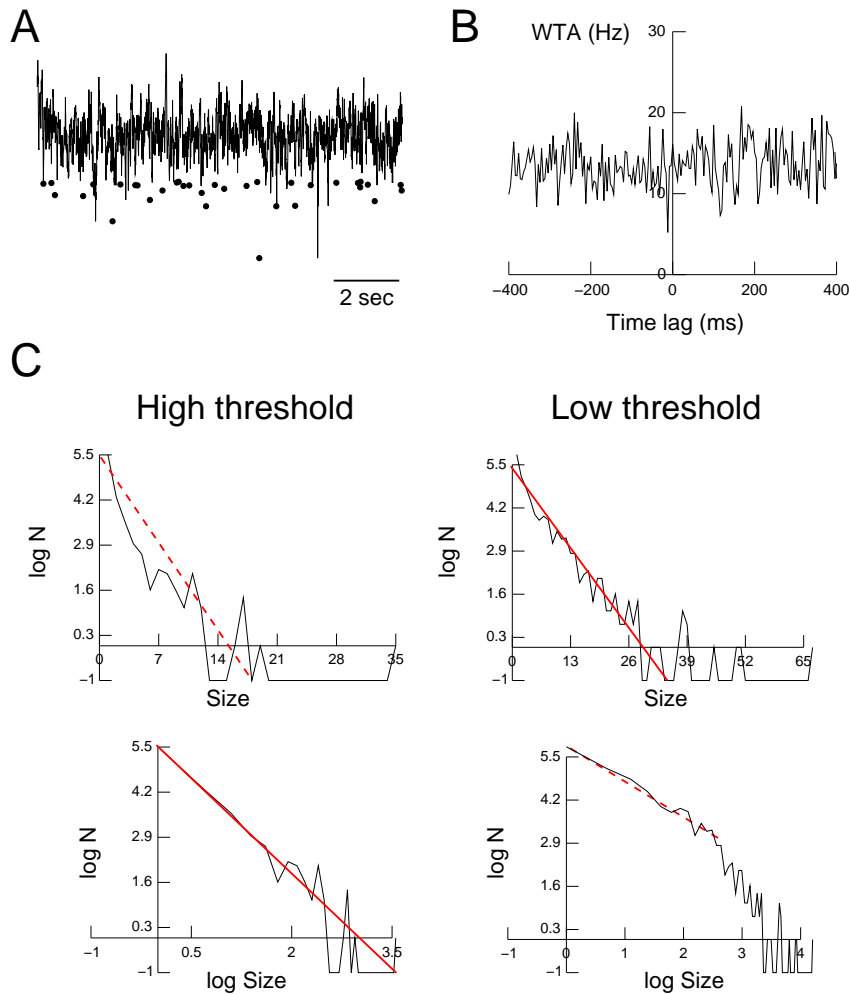


Fig. 5. Avalanche analysis from shuffled negative LFP peaks. A. Shuffled peaks obtained from randomizing the time occurrence of nLFP peaks. B. Absence of relation of shuffled peaks with unit activity. C. Scaling of avalanche peak size distribution, showing similar behavior as for nLFPs (compare with Fig. 3).

The power-law scaling of nLFP size distributions was also apparent from the peak distributions computed from single LFP channels, as illustrated in Fig. 6. To assess the significance of this result, we performed a Kolmogorov-Smirnoff test to these data. For peak amplitudes in single channels, some channels (namely channels 1,2 and 6) clearly gave a better fit to an exponential law than a power-law, but for the other channels the test was not conclusive. In those cases, although visually we are able to fit the data with a power-law, the analysis shows that neither power-law nor exponential decay provides a good fit to the data. Interestingly, the peak size distribution scales exponentially as well as a power-law (Fig. 6A-B).

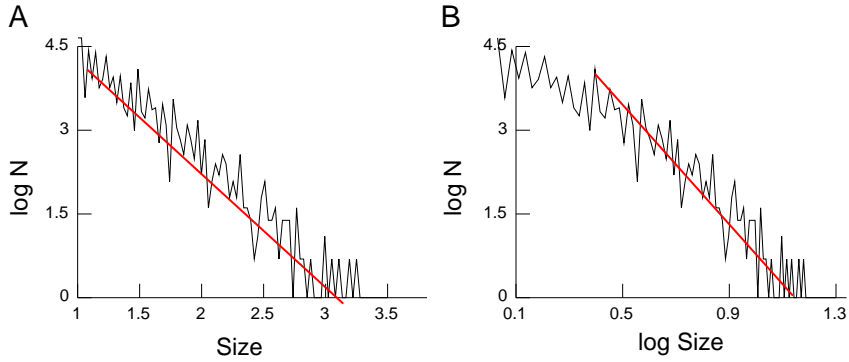


Fig. 6. Distributions of negative LFP peaks from single channels. The peak distribution is shown in log-linear (A) and logarithmic scale (B).

At this point, we conclude that a “naive” avalanche dynamics of nLFPs, based only on the scaling in log-log representations, can display power-law scaling in some cases, depending on the detection threshold used. High thresholds, which select events of exceptionally large amplitude, tend to give power-law relations. In contrast, low thresholds, which select many events, give rise to exponential distributions, similar to stochastic processes. The application of more severe statistical tests, such as the Kolmogorov-Smirnoff test, shows that the power-law relations are not supported by solid statistical grounds. The dependence on the threshold is much weaker in the statistical data analysis, as we can clearly see in Tables 1 and 2. Moreover, in agreement with this observation, an apparent power-law scaling is also seen for positive peaks and shuffled data, where the peaks are unrelated to neuronal activity. This suggests that some form of power-law scaling (as seen in log-log representations) seems not related to neuronal activity, but could rather represent a generic property of these signals. To test this hypothesis, we now turn to the analysis and simulations of stochastic processes.

Power-law scaling from stochastic processes

We first investigate computationally whether a power-law relation can be obtained from the peak size distribution of a purely stochastic process. To this end, we generate a high-frequency shot-noise process, consisting of exponential events convolved with a Poisson process. This process satisfies the equation

$$\tau_m dV_t = -V_t dt + \sum_{i=1}^P q_i dN_t^{(i)} \quad (3)$$

Table 2. Kolmogorov-Smirnoff and p-values for avalanche sizes.

Data Type and threshold	Exponential fit				Power-Law fit			
	λ	gof	p-val	%	α	gof	p-val	%
Neg. Low	0.25	0.12	0.00	4	3.28	0.06	0.025	18
Neg. High	0.26	0.12	0.00	8	1.97	0.056	0	1
Pos Low	0.27	0.18	0.00	0.42	3.5	0.13	0	0.25
Pos. High	0.35	0.17	0.00	0.12	1.95	0.084	0.00	1

Kolmogorov-Smirnoff and p-values for avalanche size, defined as the number of peaks within the avalanche, for both positive and negative events. Same variables as described in Table 1.

where τ_s is the characteristic decay time constant of each exponential event, q_i is the jump amplitude of each event, and $N_t^{(i)}$ are independent Poisson processes. The solution of Eq. (3) can be written as:

$$V_t = \sum_{i=1}^P \sum_{t^i \text{ times of } N^{(i)}} \exp\left(\frac{t - \tau_i}{\tau_s}\right). \quad (4)$$

Here, the stochastic variable V_t represents the LFP as the summation of a large number of randomly-occurring synaptic events, each described by a decaying exponential.

The peaks were detected according to a high threshold, to mimic the experimental paradigm in Fig. 6A. As for the LFP data, this procedure yielded power-law amplitude distributions, but the same distributions also scaled exponentially (Fig. 7B-C).

Peak distribution shot noise model

We now investigate this problem analytically. If the number of Poisson processes P is equal or reducible to one, the integrated process (4) simply reads:

$$V_t = V_0 e^{-t\tau_s} + q \sum_{t^{(i)} \leq t \text{ jump}} e^{-(t-t^{(i)})/\tau_s} \quad (5)$$

We are interested in the probability that the supremum of this process reaches a certain threshold value θ during an interval of times $[0, T]$. In order to compute this probability, we condition on the number of jumps of the Poisson process in this interval of time. Since the events are disconnected, we have:

$$\begin{aligned} \mathbb{P}\left(\max_{[0, T]} V_t \geq \theta\right) &= \sum_{N \in \mathbb{N}} \mathbb{P}\left(\max_{[0, T]} V_t \geq \theta \cap \mathcal{N}([0, T]) = N\right) \\ &= \sum_{N \in \mathbb{N}} \mathbb{P}\left(\max_{[0, T]} V_t \geq \theta \mid \mathcal{N}([0, T]) = N\right) \mathbb{P}(\mathcal{N}([0, T]) = N) \\ &= e^{-\lambda T} \sum_{N \in \mathbb{N}} \frac{(\lambda T)^N}{N!} \mathbb{P}\left(\max_{[0, T]} V_t \geq \theta \mid \mathcal{N}([0, T]) = N\right) \end{aligned} \quad (6)$$

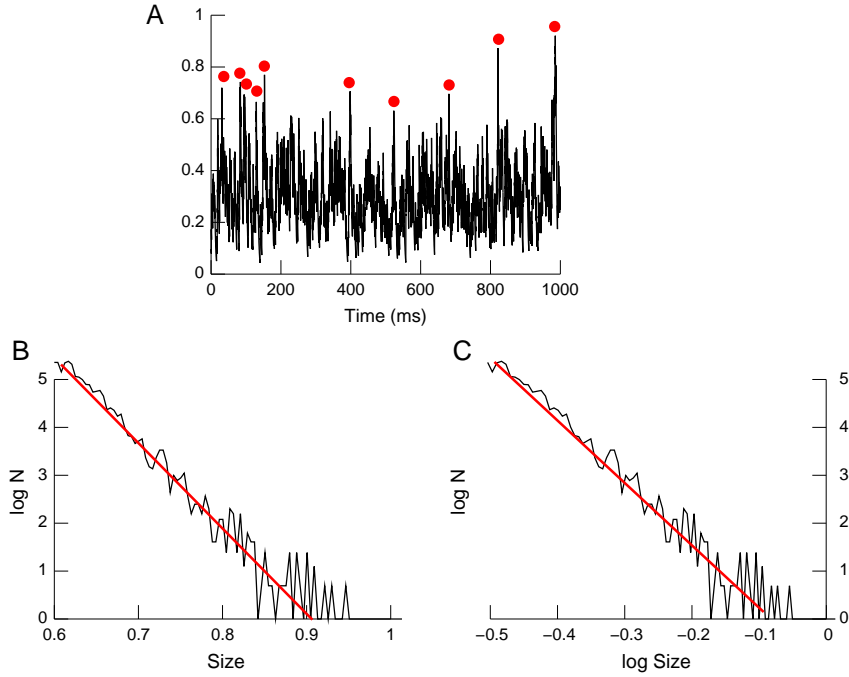


Fig. 7. Distributions of peak amplitudes from a thresholded Poisson shot-noise process. A. Stochastic process and examples of detected peaks. B. Event size distributions for the distribution of peak amplitudes in log-linear scale. C. Same distribution in logarithmic scale. Straight lines indicate the best fit using linear regression.

The maxima of this process occur at the times of the Poisson process, which we denoted $t^{(i)}$, and these local maxima have the values:

$$\left\{ \begin{array}{l} t = 0 \quad V_0 \\ t = t^{(1)} \quad V_1 := V_0 e^{-t^{(1)}/\tau_m} + q \\ t = t^{(2)} \quad V_2 := V_0 e^{-t^{(2)}/\tau_m} + q \left(e^{-(t^{(2)}-t^{(1)})/\tau_m} + 1 \right) \\ \dots \\ t = t^{(N)} \quad V_N := V_0 e^{-t^{(N)}/\tau_m} + q \left(e^{-(t^{(N)}-t^{(1)})/\tau_m} + e^{-(t^{(N)}-t^{(2)})/\tau_m} + \dots \right. \\ \quad \left. + e^{-(t^{(N)}-t^{(N-1)})/\tau_m} + 1 \right) \\ \quad = e^{-t^{(N)}/\tau_m} \left(V_0 + q \sum_{i=1}^N e^{t^{(i)}/\tau_m} \right) \end{array} \right. \quad (7)$$

Furthermore, conditionally on $\mathcal{N}([0, T])$ the number of jumps of the Poisson process in the time interval $[0, T]$, the instants of these jumps are uniformly distributed in the interval $[0, T]$. Therefore, the probability that the max is greater than the threshold θ can be written as the following integral:

$$\mathbb{P} \left(\max_{[0, T]} V_t \geq \theta \mid \mathcal{N}([0, T]) = N \right) = \int_{t^{(1)}=0}^T \int_{t^{(2)}=0}^T \dots \int_{t^{(k)}=0}^T \mathbb{1}_{\left\{ \exists k \in \{1, \dots, N\} \text{ such that } e^{-t^{(k)}/\tau_m} \left(V_0 + q \sum_{i=1}^k e^{-t^{(i)}/\tau_m} \right) \geq \theta \right\}} \frac{dt^{(1)} \dots dt^{(k)}}{T^k} \quad (8)$$

where $\mathbb{1}_A$ is the indicative function of the set A . This integral cannot be simplified further, but its numerical computation is straightforward. Therefore, the peak distribution we are searching for has the expression:

$$\mathbb{P}\left(\max_{[0,T]} V_t \geq \theta\right) = e^{-\lambda T} \sum_{N \in \mathbb{N}} \frac{(\lambda T)^N}{N!} \int_{t^{(1)}=0}^T \int_{t^{(2)}=0}^T \cdots \int_{t^{(k)}=0}^T \mathbb{1}_{\{\exists k \in \{1, \dots, N\} \text{ such that } e^{-(t^{(k)})/\tau_m} (V_0 + q \sum_{i=1}^k e^{-(t^{(i)})/\tau_m}) \geq \theta\}} \frac{dt^{(1)} \dots dt^{(k)}}{T^k} \quad (9)$$

This expression is accurately approximated using a numerical integration method and truncating the series. The approximation error is proportional to the rest of the exponential series $R(N) = \sum_{k=N+1}^{\infty} (\lambda T)^k / k!$. Simulation results of this formula are presented in Fig. 8 and predict the results obtained by numerical simulations in Fig. 7: both exponential and logarithmic distribution give a good model for the peak distribution. The Kolmogorov-Smirnov statistical fits and tests are in accordance with this observation, and are provided in Table 3.

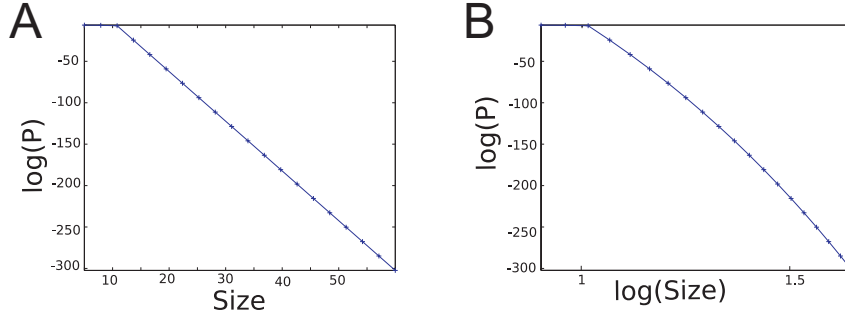


Fig. 8. Peak amplitude distribution for the Shot-Noise model. The same distribution is shown in log-linear scale (A) and in logarithmic scale (B). It presents an exponential decay for large values of θ . Simulation: intensity of the process $\lambda = 4$, $\tau_m = 2$, $V_0 = 0$, $T = 10$, $\theta = 10$, maximal value of peaks considered 25 (see text)

Let us now consider the distribution of the maxima of the process (5) conditionally on the fact that the process does an excursion above a certain threshold. This case can be treated in a similar fashion, but considering the distribution of local minima also. These local minima are reached at times $t^{(k)-}$ just before the jumps of the Poisson process, and their value are $V_{t^{(k)-}} - q$. The probability of the occurring of an excursion above θ and exceeding μ (event denoted A_θ^μ) can therefore be written as:

$$\begin{aligned} \mathbb{P}(A_\theta^\mu) &= \sum_{N \in \mathbb{N}} \mathbb{P}(A_\theta^\mu \cap \mathcal{N}([0, T]) = N) \\ &= e^{-\lambda T} \sum_{N \in \mathbb{N}} \frac{(\lambda T)^N}{N!} \mathbb{P}(A_\theta^\mu | \mathcal{N}([0, T]) = N) \end{aligned}$$

and the probability $\mathbb{P}(A_\theta^\mu | \mathcal{N}([0, T]) = N)$ can be easily evaluated numerically using the following representation:

$$\mathbb{P}(A_\theta^\mu | \mathcal{N}([0, T]) = N) = \int_{t^{(1)}=0}^T \int_{t^{(2)}=0}^T \cdots \int_{t^{(N)}=0}^T \mathbb{1}_{\{\exists k \in \{1, \dots, N\} \text{ and } l \in \{k+1, \dots, N\} \text{ such that } V_k \geq \mu, V_l \leq \theta\}} \frac{dt^{(1)} \dots dt^{(N)}}{T^N} \quad (10)$$

Table 3. Kolmogorov-Smirnoff tests for thresholded stochastic processes

Data type	Exponential fit			Power-Law fit		
	λ	gof	p-val	α	gof	p-val
Shot-Noise single-barrier	0.70	0.103	0.12	10.08	0.185	0.00
Shot-Noise excursion	0.72	0.014	1.00	15.00	0.094	0.28
Ornstein-Uhlenbeck single-barrier	2.40	0.042	0.97	44	0.077	0.62
Ornstein-Uhlenbeck excursion	2.42	0.0051	1.00	48.00	0.012	0.92

Theoretical laws: statistical fit with exponential and power-law distributions. High values of the estimated power-law parameter appears because we considered the tail of the distribution, and since the data present an exponential trend, the estimated power-law exponent becomes larger when thresholds are high. Even if the p-value is high, the fit is not realistic and the does not hold for larger intervals.

The results present the same characteristics as the case where we do not consider excursions (see Fig. 9 and Table 3).

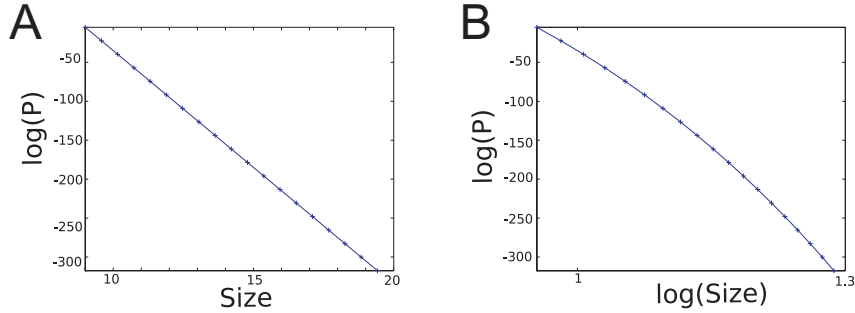


Fig. 9. Peak amplitude distribution of excursions in the Shot-Noise model. The same distribution is shown in log-linear scale (A) and in logarithmic scale (B). It presents an exponential decay for large values of θ . Simulation: intensity of the process $\lambda = 4$, $\tau_m = 2$, $V_0 = 0$, $T = 10$, $\theta = 10$, maximal value of peaks considered: 25.

Multiple Poisson Processes and Diffusion Approximation

The case where the LFP is generated by a finite number of independent Poisson processes can be treated in the same fashion, and yields to more intricate but still easily and efficiently implemented formula. The calculations straightforwardly deduced from the previous ones are not provided here for the sake of simplicity.

In the limit of a high number of Poisson processes with summable intensities (or in the limit of a finite number of Poisson process with high firing rate and suitable scaling on the jump amplitude), the solution of equation (3) converges in law towards the solution of the equation:

$$\tau_s dV_t = (\mu - V_t) dt + \sigma dW_t \quad (11)$$

where μ is related to the amplitude of the q_i and the rates of the Poisson processes $N^{(i)}$. This convergence can be proved using for instance Donsker's theorem (see e.g. Billingsley (1999); Touboul and Faugeras

(2007)) and is generally called *diffusion approximation*. The process solution of equation (11) is an Ornstein-Uhlenbeck process, and reads:

$$V_t = V_0 e^{-t/\tau_s} + \mu(1 - e^{-t/\tau_s}) + \frac{\sigma}{\tau_s} \int_0^t e^{(s-t)/\tau_s} dW_s \quad (12)$$

Since the process has the same regularity as the Brownian motion, it is nowhere differentiable, and that it has a dense countable set of local maxima. The problem is reduced in this case to the probability that the process exceeds a certain value. This probability can be deduced from the law of the first hitting time of the Ornstein-Uhlenbeck process. Indeed, let us denote by τ_a the first hitting time of the threshold a for the Ornstein-Uhlenbeck process given by equation (12). The probability distribution of the peaks greater than a certain level a satisfy the equation:

$$\begin{aligned} \mathbb{P} \left(\sup_{s \in [0, t]} V_s \geq a \mid \sup_{s \in [0, t]} V_s \geq \theta, V_0 \right) &= \mathbb{P} \left(\sup_{s \in [0, t]} V_s \geq a \mid V_0 \right) \\ &= \mathbb{P} \left(\tau_a \leq t \mid V_0 \right) \end{aligned} \quad (13)$$

The excursion case continuous equivalent consists in considering the probability of exceeding a certain quantity a before going back under the excursion threshold θ . This probability can be written as:

$$\begin{aligned} \mathbb{P} \left(\sup_{s \in [0, t]} V_s \geq a, \inf_{t \in [\tau_a, t]} V_s \leq \theta \mid \sup_{s \in [0, t]} V_s \geq \theta, V_0 \right) &= \mathbb{P} \left(\sup_{s \in [0, t]} V_s \geq a, \inf_{t \in [\tau_a, t]} V_s \leq \theta \mid V_0 \right) \\ &= \int_{s=0}^t \mathbb{P} \left(\tau_\theta \leq t \mid V_s = a \right) \mathbb{P} \left(\tau_a \in ds \mid V_0 \right) \end{aligned} \quad (14)$$

Therefore the repartition function of the maxima and of maxima above a certain threshold can be deduced from the repartition function of the first hitting time of the process V . As reviewed in Alili et al. (2005); Touboul and Faugeras (2007), there is no closed form solution for the probability distribution of these hitting times, but they can be efficiently computed numerically. The most convenient solution consists in solving a Volterra integral equation giving the first hitting time of this law (see e.g. Schrodinger (1915); Plesser (1999); Touboul and Faugeras (2007)). The full distribution of the maximum is a mono-modal distribution. Here again, the same remarks are valid: we observe (see Fig. 10) that one cannot distinguish between power-law or exponential law for the peak distribution.

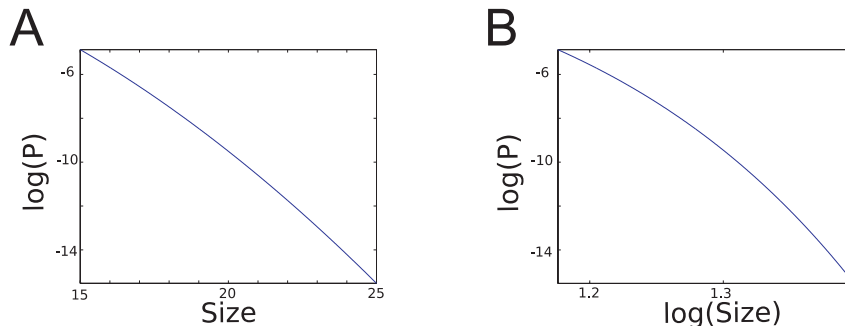


Fig. 10. Peak amplitude distribution in the Ornstein-Uhlenbeck model. The same distribution is shown in log-linear scale (A) and in logarithmic scale (B). It presents an exponential decay for large values of θ . Simulation: $\mu = 0$, $\tau = 1$, $\sigma = 4$, $t = 10$, $\theta = 10$, maximal value of peaks considered: 25.

This analysis therefore confirms that thresholded stochastic processes can display a power-law scaling, but only when performing simple line fitting in log-log representations. Indeed, we observe that it is always possible to fit a power-law distribution to the tail of the distribution with a quite good agreement, but these fit do not hold for large values of threshold (see Table 3). As a general remark, estimated laws yield high values of the exponent which is not very realistic in general. This is consistent with the findings reported above for LFPs: the power-law scaling of LFP peaks displays very similar properties to that of stochastic processes, which supports the idea that such power-law scaling is not related to neuronal activity, but may be explained by a generic property of thresholded stochastic processes. We conclude that the power-law scaling, in particular as deduced from log-log representations, does not constitute a proof of self-organized criticality, but should be complemented by other more sophisticated statistical analyses.

Discussion

In this paper, we have provided an analysis of multisite LFP recordings in awake cats, and used the detection of negative LFP peaks (nLFPs), as done in a previous study (Petermann et al. 2009). The analysis shows that the time occurrences and amplitudes of nLFPs can show power-law distributions, but only when the detection threshold is relatively high, so that only large nLFPs are selected. Lowering the threshold leads to exponential distributions. Interestingly, while nLFPs were clearly related to neural events, very similar results were obtained from positive LFP peaks, which are not statistically related to neuronal spiking activity. Moreover, the same conclusion applies after random shuffling of LFP peak times, which is analogous to a stochastic process.

In agreement with these findings, we also found seemingly power-law scaling from stochastic processes. To this end, we used two different simple stochastic models to analyze the amplitude of the nLFPs, one corresponding to LFPs arising from a linear summation of spikes arriving at the times of a Poisson process (a shot-noise process) and the diffusion limit of this phenomenon, resulting in an Ornstein-Uhlenbeck process. The former case can be solved in a closed form while the latter case is solved using the laws of the first hitting times of the Ornstein-Uhlenbeck process. Both cases present the same indeterminacy when only looking at the log-linear and log-log plots, and both power-laws and exponential laws can be fitted. However, the application of a more severe statistical test, the Kolmogorov-Smirnoff test, demonstrated that some apparent power-law scaling (as seen from log-log representations) is not supported by solid statistical grounds, in real data as well as in the theoretical laws computed, in agreement with previous studies (see e.g. Clauset et al. (2009)).

Thus, contrary to a previous study in monkey (Petermann et al. 2009), where the same controls were not done, our analysis suggests that the power-law scaling is not related to neuronal activity in awake cats. This is in agreement with a previous analysis (Bedard et al. 2006) which failed to see evidence for power-law distributions and avalanche dynamics from spiking activity, which rather scaled exponentially. However, there is still the possibility that cats and monkey display fundamental differences, or that the different brain areas or cortical layers used in these experiments also explain the differences. Further studies should address these points.

Acknowledgments

Research supported by the NSF (grant DMS0817131), CNRS, ANR and the European Community (FACETS project).

References

Alili, L., Patie, P., and Pedersen, J. L. (2005). Representations of the first hitting time density of an Ornstein-Uhlenbeck process. *Stochastic Models*, 21:967–980.

-
- Arnold, B. (1983). *Pareto distributions*. International Co-operative Pub. House.
- Barndorff-Nielsen, O. E. and Cox, D. R. (1995). *Inference and Asymptotics*. Chapman and Hall, London.
- Bedard, C., Kroger, H., and Destexhe, A. (2006). Model of low-pass filtering of local field potentials in brain tissue. *Phys Rev E Stat Nonlin Soft Matter Phys*, 73(5 Pt 1):051911.
- Beggs, J. M. and Plenz, D. (2004). Neuronal avalanches are diverse and precise activity patterns that are stable for many hours in cortical slice cultures. *J Neurosci*, 24(22):5216–5229.
- Billingsley, P. (1999). *Convergence of Probability Measures*. Wiley series in probability and statistics.
- Clauset, A., Shalizi, C. R., and Newman, M. (2009). Power-law distributions in empirical data. arXiv.org:0706.1062.
- Destexhe, A., Contreras, D., and Steriade, M. (1999). Spatiotemporal analysis of local field potentials and unit discharges in cat cerebral cortex during natural wake and sleep states. *J Neurosci*, 19(11):4595–4608.
- Jensen, H.J. (1998) *Self-Organized Criticality. Emergent Complex Behavior in Physical and Biological Systems*. Cambridge University Press, Cambridge UK.
- Muniruzzaman, A. (1957). On measures of location and dispersion and tests of hypotheses on a pareto population,” *Bulletin of the Calcutta Statistical Association*, 7:115–123.
- Petermann T, Thiagarajan TC, Lebedev MA, Nicolelis MA, Chialvo DR, and Plenz D. (2009). Spontaneous cortical activity in awake monkeys composed of neuronal avalanches. *Proc. Natl. Acad. Sci. USA*, in press.
- Plesser, H. E. (1999). *Aspects of signal processing in noisy neurons*. PhD thesis, Georg-August-Universität.
- Schrodinger, E. (1915). Zur theorie der fall-und steigversuche an teilchen mit brownscher bewegung. *Physikalische Zeitschrift*, 16:289–295.
- Steriade, M. (2001) Impact of network activities on neuronal properties in corticothalamic systems. *J. Neurophysiol.* 86: 1–39.
- Stoev, S., Michailidis, G., and Taqqu, M. (2006). Estimating heavy-tail exponents through max self-similarity. *Arxiv preprint math.ST/0609163*.
- Touboul, J. and Faugeras, O. (2007). The spikes trains probability distributions: a stochastic calculus approach. *Journal of Physiology, Paris*, 101/1-3:78–98.